Current Otorhinolaryngology Reports (2020) 8:120–128
https://doi.org/10.1007/s40136-020-00277-8

SKULL BASE SURGERY (CH SYNDERMAN AND EW WANG, SECTION EDITORS)

Imaging of Anterior and Central Skull Base Tumors: a Review

Christopher M. Low[1] · Jamie J. Van Gompel[2] · Garret Choby[1]

Published online: 13 March 2020

Abstract

Purpose of Review The aim of this review is to summarize characteristic imaging findings of common skull base lesions. In addition, this study aims to review the literature regarding important and interesting new advancements in imaging of the anterior and central skull base.

Recent Findings Imaging techniques including magnetic resonance elastography, indocyanine green fluorescence, Gallium-DOTATATE PET/CT, peptide receptor radionucleotide therapy, and 3D printing are being used to advance the care of patients with skull base pathology.

Summary Characteristic CT and MRI findings can be used to narrow the differential diagnosis and plan treatment for anterior and central skull base lesions. New imaging techniques show promise in improving the care of patients with skull base lesions.

Keywords Anterior skull base imaging · Endoscopic skull base surgery · Magnetic resonance elastography · Indocyanine green fluorescence · Gallium-DOTATATE PET/CT · 3D printing · Extended endonasal approach

Introduction

The skull base is a complex anatomic region at the intersection of the sinonasal cavity, orbits, and anterior/middle cranial fossa. The anterior skull base extends from the posterior table of the frontal sinus to the anterior clinoid processes [1] while the central skull base makes up the floor of the middle cranial fossa and is comprised of the sella and clivus in the midline sagittal plane [2]. Tumors of the anterior and central skull base are heterogeneous including neoplasms that are neurogenic, chondro-osseous, and sinonasal in origin. Imaging of skull base tumors is helpful in narrowing a differential diagnosis, and characterizing the extent of a lesion to create a treatment plan. In operative planning, imaging plays a critical role in treatment planning by elucidating the relationship of the mass with critical neurovascular structures. Finally, it is also useful in post-operative assessment and surveillance of recurrence.

Computed tomography (CT) and magnetic resonance imaging (MRI) are complementary modalities and serve as the workhorse imaging studies for visualizing the anterior and central skull base. Obtaining pre-operative imaging allows for better characterization of disease and allows for intraoperative stereotactic guidance and navigation [3•]. CT provides improved bony anatomic detail and distinctly shows presence of bony invasion and remodeling, and calcification, and identifies fibro-osseous lesions. In contrast, MRI is superior in illustrating soft tissue pathologic conditions and illustrating extent of disease. This includes delineating the soft tissue–tumor interface and better illustrating the extent of invasion into nearby structures such as the dura or brain parenchyma, the orbit, or cavernous sinus. Finally, a discussion about tumors is not complete without mention of non-neoplastic sinonasal etiologies such as allergic fungal sinusitis, fungal ball or mycetoma, and mucocele. These entities are important to keep on the differential diagnosis as they can mimic neoplasm and even be a concurrent finding in the context of neoplasm. MRI is helpful in distinguishing tumor from these non-neoplastic entities and will be briefly covered in this review. Angiography, including CT angiography or time-of-flight MR angiography, helps define the relationship of the

This article is part of the Topical collection on *Skull Base Surgery*

✉ Garret Choby
Choby.Garret@mayo.edu

Christopher M. Low
Low.Christopher1@mayo.edu

Jamie J. Van Gompel
VanGompel.Jamie@mayo.edu

[1] Department of Otolaryngology-Head and Neck Surgery, Mayo Clinic, 200 First St SW, Rochester, MN 55905, USA

[2] Department of Neurologic Surgery, Mayo Clinic, Rochester, MN 55905, USA

mass with important vascular structures and assists in characterizing the blood supply to hypervascular tumors. This is especially useful when addressing pathology in close proximity to the internal carotid artery and basilar artery systems. Additional studies can be utilized as clinically indicated and in unique circumstances. Recent findings include use of special imaging protocols and novel uses of existing technology in a unique way to give the clinician additional information. This includes the use of MR elastography, indocyanine green fluorescence, Gallium-DOTATATE, peptide receptor radionucleotide therapy, and 3D printing.

The purpose of this review is to discuss the differential diagnosis, and characteristic imaging findings of common skull base lesions. In addition, this review emphasizes interesting new findings and aims to bring the reader up-to-date on imaging of the anterior and central skull base.

Technical Considerations

All skull base imaging including CT and MRI should be obtained with small slice thickness because of the small size of neurovascular structures being studied and the varying course of the skull base. CT is typically obtained in 0.5–1-mm slice thickness in bone and soft tissue algorithms and reconstructed in multiple planes. Contrast-enhanced CT imaging can be used to clearly delineate vascular structures and help better characterize a mass. MRI should be obtained in small slice thicknesses as well, typically ≤ 3 mm. The sequences obtained in a skull base protocol can vary by institution but typically include at minimum T1, T2, and post gadolinium contrast T1 sequences. Additional sequences can be utilized in the study including high-resolution T2 constructive interference in steady-state (CISS), diffusion-weighted imaging, and STIR (short tau inversion recovery) [4]. Different sequences can be utilized to study different aspects of the tumor-specific properties. T1-weighted imaging may reveal bone marrow invasion and is excellent for showing presence or loss or fat or melanin. T2-weighted imaging demonstrates the CSF interface with surrounding structures, mucosal structures in the paranasal sinuses, and the water content of skull base lesions. T2 CISS uses CSF as a contrast agent to demonstrate cranial nerves and vessels. In other imaging manufacturers, this sequence may be called FIESTA or T2*. T1 post gadolinium is most sensitive in identifying perineural spread and can differentiate tumor from peripherally enhancing inflammatory sinonasal disease. On diffusion-weighted imaging (DWI), malignant tumors tend to have more restricted diffusion than benign disease with the exception of cholesteatoma and epidermoid cysts. STIR may reveal bone marrow invasion and may show metastatic lymph nodes. Post-contrast imaging that utilizes fat suppression may have limited utility in the skull base as there is a potential risk of incomplete fat suppression mimicking tumor enhancement. It should be noted that more is not necessarily better in MRI when the tesla power is concerned, 3-T exams introduce artifact at the skull base and most often imaging is perhaps even better with 1.5-T resolution imaging as this minimizes the effect of air and bone at the skull base for tumors. [5]

Anterior Skull Base Tumors

Anatomy of the Anterior Skull Base

The anterior skull base is the junction of the anterior cranial fossa and what lies inferior—the sinonasal cavity and orbits. At the center of the anterior skull base is the cribriform plate which houses the olfactory groove and allows transmission of the olfactory nerves from the olfactory blub cranially to the nasal cavity caudally. Extending out peripherally, the anterior skull base is made up of the posterior table of the frontal sinus anteriorly and the sweeps back to the anterior clinoid processes posteriorly. The lateral limits are the orbital plates of the frontal bone.

Differential Diagnosis of Lesions of the Anterior Skull Base

The differential diagnosis for anterior skull base tumors is wide and includes neoplastic and non-neoplastic etiologies. Neoplastic lesions of the anterior skull base can be classified by location of origin. Some originate inferiorly in the sinonasal cavity or orbit and extend intracranially, some can be intrinsic to the bone of the skull base, and others originate superiorly and be neurogenic in origin. Non-neoplastic entities include post-obstructive insipissated secretions, mucocele, fungal ball, and infectious etiologies including abscess or even invasive fungal rhinosinusitis.

Imaging Characteristics of Anterior Skull Base Tumors

Imaging characteristics of pertinent tumors and lesions of the anterior skull base are listed in Table 1 [6–9]. Imaging of chondro-osseous tumors is covered in the discussion of imaging of the central skull base.

Relative to the skull base, inferiorly based malignant neoplasms are typically sinonasal in origin. They are diverse and include squamous cell carcinoma, lymphoma, adenoid cystic carcinoma, and esthesioneuroblastoma (ENB), amongst others. Squamous cell carcinoma is the most common sinonasal malignancy. Bone window CT may show erosion of bone and MRI may show solid enhancement and intermediate to low T2 signal. Other common malignancies such as lymphoma and adenocarcinoma will have non-specific imaging features. Adenoid cystic carcinoma, which has perineural

Table 1 Imaging characteristics of anterior skull base lesions

	Lesion	CT	MRI	Distinguishing features
Inferiorly based—sinonasal or orbital origin				
Malignant neoplasms	Squamous cell carcinoma	• Evaluate for bone invasion which may appear as lysis on bone window	• Intermediate to low T2 signal is a sign of cellularity • Solid enhancement (in contrast to benign mucosal disease)	• Non-specific imaging features
	Adenocarcinoma	• May have bony destruction and invasion of nearby structures • Heterogeneous contrast enhancement	• Intermediate T1 and T2 signal • Possible high-intensity hemorrhagic foci	
	Adenoid cystic carcinoma		• Usually T2 intermediate signal • Low-grade lesions can by T2 hyperintense like inflammatory disease	• Assess for perineural spread
	Sinonasal mucosal melanoma		• Early on, may remodel bone in benign appearing manner • T1 hyperintense	• Often arise from nasal septum or turbinate
	Olfactory neuroblastoma	• May have small peripheral cysts and calcifications	• Intermediate T1 • Mild T2 hyperintensity • Avid homogenous enhancement due to hypervascularity	• Often found in olfactory groove • Bony destruction may distinguish from meningioma • "Dumbbell shape"
Benign neoplasms	Inverted papilloma	• Soft tissue density mass • Focus of hyperostosis • MAY have bony resorption • Lobulated and stalked from the bone	• T1 isointense • T2 alternating hypo and hyperintense • Heterogeneous enhancement	
	Juvenile nasopharyngeal angiofibroma		• T1 hypointense • T2 intermediate signal • Avid enhancement • Internal flow voids • Extension into the pterygopalatine fossa	• Adolescent male • Angiography helps characterize vascular supply • Arising from primitive vascular tissue at SPA foramen
Benign sinonasal disease	Mucocele	• Opacified sinus • Thinning of the sinus walls • Round expansile appearance	• Depends on if protein or water rich content • Protein rich: T1 hyperintense and T2 hypointense	
	Allergic fungal rhinosinusitis	• Hyperdense opacification • Expansion, remodeling, and thinning of involved sinus walls	• No contrast enhancement of the middle of sinus contents • T1 hypointense • T2 hypointense	
	Fungal ball	• Soft tissue density, foci of hyperdense deposit	• No contrast enhancement of the middle of sinus contents • T1 hypointense • T2 hypointense	• Often unilateral with single sinus involvement
Superiorly based—neurogenic origin				
Benign neoplasms	Meningioma	• Hyperostosis • Hyperattenuating to brain in 75%	• Variable—may be T1 and T2 isointense • Avid contrast enhancement Enhancing dural tail	
	Schwannoma	• Intense contrast enhancement • Smooth remodeling of adjacent bone	• T1 isointense to hypointense • Heterogeneous enhancement • May have cystic structures	

spread as a characteristic feature, may show enhancement of peripheral nerves on MRI. ENB shows heterogeneous contrast enhancement due to hypervascularity and mild T2 hyperintensity. These lesions are found in the olfactory groove, may exhibit bony destruction in contrast to meningioma, and may have a "dumbbell shape" if it has both intracranial and sinonasal extension.

Benign neoplasms of the sinonasal cavity include inverted papilloma (IP) and juvenile nasopharyngeal angiofibroma (JNA). When evaluating an adolescent male with recurrent epistaxis, the clinician should have a suspicion for JNA (Fig. 1a). Characteristic imaging features of this entity include a mass or lesion arising from the sphenopalatine foramen with MRI showing internal flow voids, avid enhancement, and T1 hypointensity. The "Holman-Miller" sign refers to the widening of the pterygopalatine fossa and anterior bowing of the posterior maxillary sinus wall from the JNA. IP will show a mass with soft tissue density on CT imaging. CT may also reveal a focus of hyperostosis which suggests the point of attachment of the lesion. On MRI, IP will be T1 isointense and show heterogeneous enhancement.

Benign sinonasal disease can present unilaterally and mimic a neoplastic process. However, they have their own imaging features and careful review of these lesions can often separate them from a true neoplastic process. Fungal ball or mycetoma can present as opacification of a single, unilateral sinus—most commonly the maxillary sinus but also in the sphenoid sinus. Characteristic imaging features include CT soft tissue heterogeneity with characteristic hyperdensities from iron elements. Allergic fungal rhinosinusitis will show hyperdense material on CT and can show expansion and even remodeling of and thinning of involved sinus walls. T1- and T2-weighted sequences on MRI will be hypointense and while the mucosal lining will show gadolinium enhancement, the center of the sinus contents will no show enhancement, in contrast to neoplasms. A mucocele will show complete opacification of a sinus, expansile thinning of walls on CT. MRI findings depend on if the contents are rich in protein or water. If rich in water, the contents will be T1 hypointense and T2 hyperintense but if rich in protein, the contents will be T1 hyperintense and T2 hypointense.

Neurogenic tumors are superiorly based and in the anterior skull base, meningioma, and schwannoma are high on the differential. With a meningioma, hyperostosis may be noted on CT. On MRI, these lesions show avid contrast enhancement with dural tails and T1 and T2 isointensity (Fig. 1b). Schwannoma will show smooth remodeling of adjacent bone and intense contrast enhancement on CT. MRI will show T1 isointensity to hypointensity, and heterogeneous enhancement, and may have cystic structures.

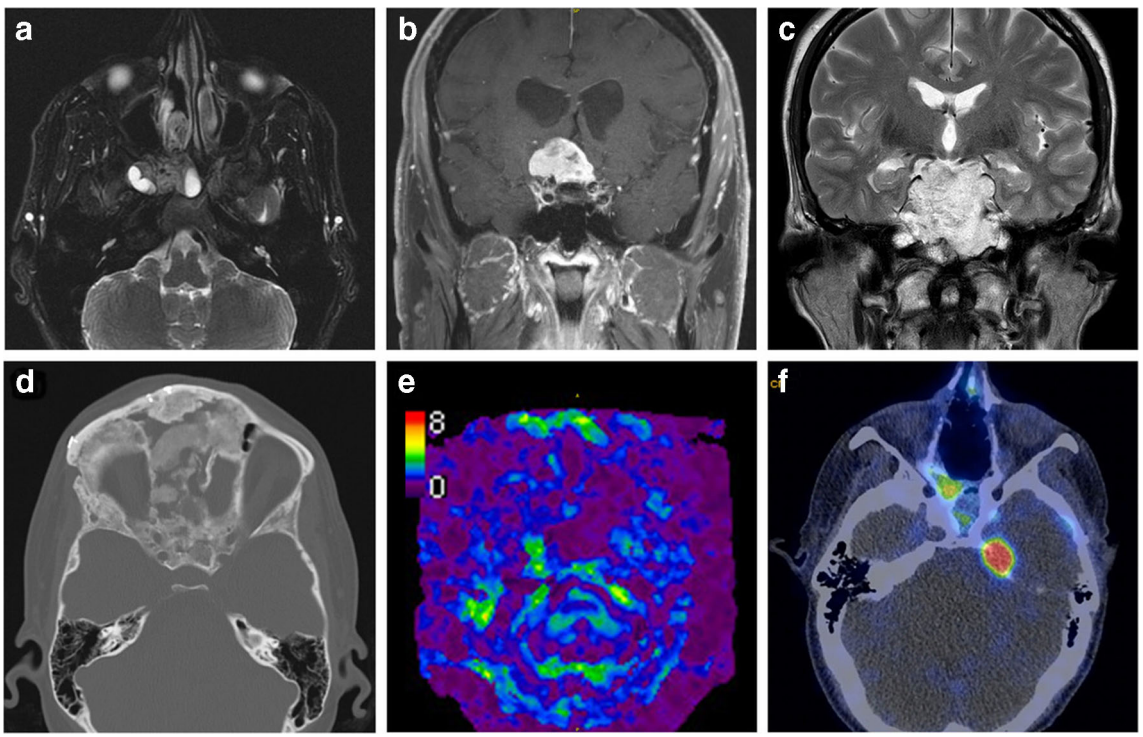

Fig. 1 **a** Juvenile Nasopharyngeal Angiofibroma. Axial T2 MRI with fat suppression shows T2 intermediate signal and internal flow voids. Extension into the pterygopalatine fossa is seen. **b** Planum sphenoidale meningioma showing avid contrast enhancement and enhancing dural tail on coronal T1-weighted MRI with gadolinium. **c** Chordoma. Coronal T2-weighted MRI shows a lobulated, heterogeneously hyperintense tumor. **d** Fibrous dysplasia. Axial CT soft tissue window shows ground glass appearance and mixed areas of sclerosis and lucency. **e** Pituitary adenoma. MR elastography shows a soft tumor. **f** Axial Gallium-Dotatate PET/CT in the setting of metastatic esthesioneuroblastoma showing multiple foci of somatostatin avid disease in the skull base and left temporal lobe

Central Skull Base Tumors

Anatomy of the Central Skull Base

The central skull base makes up the floor of the middle cranial fossa [4]. It contains the sella turcica and clivus at its center, and laterally, it includes the petrous ridge and temporal bones. The central skull base is a portal for the passage of critical neurovascular structures to and from the cranial cavity through structures such as the optic canal, superior orbital fissure, foramina rotundum, ovale and spinosum, cavernous sinus, vidian canal, and carotid canal.

Differential Diagnosis of Central Skull Base Tumors

Like the anterior skull base, the differential diagnosis for lesions of the central skull base is wide and can be classified by location of origin. Neurogenic lesions including sellar-based lesions can originate superiorly in the cranial cavity. A number of chondro-osseous bone lesions can arise from the skull base. Uniquely, the primitive notochord courses through this area and can give rise to chordomas, most commonly of the clivus. Inferiorly, nasopharyngeal carcinoma may be found along with benign and malignant pathologies of the sinonasal cavities.

Imaging Characteristics of Central Skull Base Tumors

Imaging characteristics of pertinent tumors and lesions of the central skull base are listed in Table 2 [10–12].

Sella-based lesions include pituitary microadenomas, which on MRI will have reduced gadolinium signal compared to normal gland. In addition, it may show low T1 signal and variable T2 signal. A pituitary macroadenoma may show a "snowman" morphology if extending to the suprasellar compartment. A craniopharyngioma may show calcifications and a cystic–solid component on CT while there may be low T1 signal on MRI.

Chordomas arise from the primitive notochord and are locally invasive neoplasms that demonstrate erosion and destruction within the clivus. They are technically considered to be malignant, although the risk of metastasis is very low. On CT, they show local bony destruction and sometimes calcification intrinsic to the tumor, commonly at the midline clivus. MRI shows a mass with heterogeneous enhancement and high T2 signal (a hallmark of Chordoma) (Fig. 1c).

There are a variety of chondro-osseous lesions of the skull base. An osteoma may show a single focus of sclerotic bone while an osteosarcoma will show a mixture of lysis and sclerosis on CT and a variable MRI signal depending on extent of mineralization. It will show less contrast enhancement than a chondrosarcoma, which has low T1 signal and high T2 signal. Many of the features will overlap with a chordoma but only a chondrosarcoma will clearly spare the clivus, tending to arise off midline near the petroclival junction, often with a chondroid matrix. Fibrous dysplasia will show a ground glass appearance on CT and low T1 and T2 signal on MRI (Fig. 1d).

Recent Findings

Recent advancements have been made in imaging of the anterior skull base specifically in the techniques of MR elastography, indocyanine green fluorescence, Gallium-DOTATATE, peptide receptor radionucleotide therapy, and 3D printing, which will be reviewed here.

MR Elastography

Magnetic resonance (MR) elastography is a technique by which imaging is used to assess the mechanical properties of soft tissue, specifically how soft or firm a tissue may be and also may be able to tell us if something is adhered to a neighboring structure [13]. With the ability to assess the mechanical qualities of tissue, MR elastography can be thought of as the imaging equivalent to palpation or "palpation by imaging." Applications of this imaging technique have been explored in imaging pathologies of the breast, liver, skeletal muscle heart, and brain. In the breast, this technique has shown promise in helping to improve breast cancer diagnosis in patients who have mammographically dense breast cancer tissue where usual screening imaging techniques have a more limited role [13]. In the liver, hepatic MR elastography has been pursued as one of the tools for evaluating fibrosis and has been shown to perform as well or better to transient ultrasound elastography by capturing a wider field of view, and not being limited by anatomic factors such as ascites or obesity [13].

The protocol for MR elastography starts by first providing some sort of stress or motion that deforms the tissue. For example, an acoustic frequency from an internal source such as the heartbeat, or patient humming or an external source in the form of pneumatically powered actuators, and piezoelectric bending elements have been used. Next, the tissue is imaged using a sequence that synchronizes to the frequency of the motion or stress that was given to the patient. Finally, an algorithm is used to generate and display images that give a representation of the mechanical properties of the tissue in question (Fig. 1e).

A study at our institution showed the ability to measure pituitary tumor density using MR elastography [14••]. This study proposed potential utility in pre-operative assessment of pituitary tumors prior before transsphenoidal resection of a pituitary tumor. Knowing the density of a pituitary tumor will alert the pituitary surgeon to potentially more difficult cases where tumors are not soft and suctionable and allow the surgeon to make a surgical plan accordingly by preparing more time for the case or discuss a higher risk profile with the patient.

Table 2 Imaging characteristics of major central skull base lesions

	Lesion	CT	MRI	Notes
Sella-based lesions				
Benign	Pituitary microadenoma		• Low T1 signal • Increased T2 signal • Compared to normal gland—reduced enhancement	• Dynamic post-contrast imaging—shows altered contrast uptake in the tumor in equivocal imaging
	Pituitary macroadenoma	• Moderate contrast enhancement • Expanded sella	• T1 and T2 isointense • Moderate to bright enhancement • Larger lesions may be heterogeneous due to cystic or necrotic areas	• "Snowman" morphology if extending to suprasellar compartment • Rarely narrow the cavernous carotid
	Craniopharyngioma	• Calcifications Cystic—solid appearance	• Calcifications • T1 signal shortening secondary to proteinaceous content	• Arising from remnants of Rathke's pouch
Other neurogenic				
Malignant	Chordoma	• Bony destruction—erosion of cortical margins and replacement of bone marrow of the clivus	• T1 isointense to hypointense • T2 hyperintense • Lobulated • Heterogeneous enhancement	• Expansile clival tumor • Histologically benign but locally invasive neoplasm • Arises from primitive notochord
Benign	Schwannoma	• Intense contrast enhancement • Smooth remodeling of adjacent bone	• T1 isointense to hypointense • Heterogeneous enhancement • May have cystic structures	
Chondro-osseous				
Benign	Fibrous dysplasia	• Ground glass appearance • Mixed areas of sclerosis and lucency	• Low T1 signal • Low T2 signal	• Polyostotic disease may occur with McCune-Albright
	Osteoma	• May have dense bone • Mature osteoma may resemble normal bone with marrow		
Malignant	Osteosarcoma	• Mixture of lysis and sclerosis • Cloudy or clustered mineralization	• Variable MR signal depending on mineral content • Low T1 signal • Intermediate T2 signal • Less enhancement than chondrosarcoma	• Sunburst pattern
	Chondrosarcoma	• Well differentiated: punctuate or curvilinear mineralization secondary to chondroid matrix	• Low T1 signal • High T2 signal • Relatively avid enhancement	• Increase in bone destruction with tumor grade • Often found at the petroclival synchondrosis, likely from rests of embryonal cells • Imaging features often overlap with chordoma; however, chondrosarcoma typically occurs off midline in close proximity to the aforementioned petroclival synchondrosis.

Indocyanine Green Fluorescence

Indocyanine green (ICG) angiography is an imaging technique where [15] a near-infrared fluorescent dye (C43H47N2NaO6S2) is used for visualization of vascular structures as well as perfusion. In 1959, it was approved by the Food and Drug Administration for liver diagnostic and cardiocirculatory diagnostic uses. It has since found wide use in neurologic surgery and is finding growing application in the field of endoscopic skull base surgery. A few applications are highlighted here.

ICG is injected intravenously and remains in the intravascular space by binding to large plasma proteins. This dye is exclusively processed by the liver and has a plasma half-life of 2.5 min and is not metabolized by the body. While the maximum absorption wavelength in water is 780, the binding of the dye to serum proteins cause a spectral shift that causes the florescence in blood to be at a wavelength of 820 nm. Different manufacturers have endoscope-integrated indocyanine green fluorescence systems that include a light source that at the excitation wavelength of the dye and a light filter that allows passage of near-infrared light at the emission wavelength of ICG.

In endoscopic skull base surgery, ICG has been used to identify critical vascular structures, and to potentially identify normal pituitary tissue from neoplastic tissue; however, this is in its infancy. Hide et al. utilized an ICG endoscope system to identify the internal carotid artery and patent cavernous sinus in real time [16••]. They suggested that by having real-time visualization of the vasculature supplying the pituitary gland will help to preserve the function of the pituitary gland. Litvack et al. and Verstegen et al. took intraoperative visualization of the pituitary gland a step further and utilized endoscopy with ICG fluorescence to distinguish normal pituitary gland from pathologic [15, 17] In addition, they hypothesized the use of it in identifying dural invasion. Kerr et al. utilized ICG fluorescence to identify the nasoseptal artery when harvesting the nasoseptal flap [18]. While intraoperative Doppler has historically been used to approximate the location of the nasoseptal artery, it provides poor spatial resolution. In the setting of revision surgery, ICG fluorescence can be helpful in verifying that the nasoseptal artery has not been compromised in a previous procedure and that the nasoseptal flap is still viable. This will allow the surgeon to appropriately modify the surgical plan and harvest alternate flaps or grafts if needed. Lavigne et al. utilize the ICG endoscope system to visualize the internal maxillary artery in the pterygopalatine fossa, allowing for proximal vascular control during endoscopic skull base surgery [19].

While the localization of ICG is not specific to the intravascular space, Cho et al. discussed use of tumor specific dyes, specifically OTL38, a folate analog that is conjugated to an analog of ICG. The idea is that for adenomas with high folate receptor expression, the dye will be able to help identify tumor margins intraoperative [20].

^{68}Gallium-DOTATATE and Peptide Receptor Radionucleotide Therapy with 177Lu-DOTATATE

1,4,7,10-Tetraazacyclododecane-1,4,7,10-tet-raacetic acid (DOTA)–octreotate (DOTATATE) is a somatostatin analog that can be used in conjunction with radiodyes such as gallium for diagnosis and characterization of neuroendocrine tumors such as ENB (Fig. 1f). It can also be used in conjunction with radionucleotides such as ^{177}Lutetium to treat neuroendocrine tumors as part of peptide receptor radionucleotide therapy.

Somatostatin receptors (SSTRs) are present on the surface of neuroendocrine cells and provide a biologic target for imaging and treatment. While somatostatin is the peptide hormone that largely binds this receptor and is responsible for its physiologic functions, it has been found that octreotide, a synthetic somatostatin receptor analog, also binds SSTRs. Early use of this relationship for imaging occurred in 1983 when octreotide was first radiolabeled with 111In and imaged using a nuclear medicine gamma camera [21••]. This was the beginning of the use of conjugated somatostatin analogs in diagnostic imaging and therapeutic management.

In the present day, Dotatate is conjugated to Gallium 68 (^{68}Ga) and used in positron emission tomography (PET)/computed tomography (CT). In contrast to prior nuclear imaging using gamma camera, Gallium-DOTATATE PET/CT provides superior anatomic detail and correlation [21••]. Gallium 68 has a short half-life of 68 min, and a PET/CT is performed 45–60 min after the injection of the radiotracer. With this protocol, Gallium-DOTATATE PET/CT allows for whole body imaging of somatostatin receptors and detail characterization of neuroendocrine tumors [21••]. In the skull base, Gallium-DOTATATE can be used for diagnosis of neuroendocrine tumors including ENB [22]. In addition, this modality allows for further characterization of a mass found on MRI which can allow a clinician to confidently diagnose or exclude a neuroendocrine tumor when there is high enough suspicion [23].

DOTATATE that is conjugated to radioneucleotides may be helpful in treatment of ENB in the form of peptide receptor radionucleotide therapy (PRRT). It has been used in standard practice in other neuroendocrine tumors; however, its routine use has not been established for ENB. Czapiewski et al. found that ENB express the somatostatin 2a receptor frequently and is a target for PRRT [24]. DOTATATE can be conjugated with ^{177}Lutetium to be ^{177}Lu-DOTATATE. Several case reports describe the treatment of ONB using ^{177}Lu-DOTATATE [21••, 23, 24, 25–27]. Schneider et al. found that histologically, treatment with ^{177}Lu-DOTATATE results in radiation necrosis [26]. Makis et al. describe use of both 111In-octreotide over 8 months and 3 treatments of 177Lu-DOTATATE to improve tumor symptoms. However, this treatment did not result in disease control [25]. Sabongi et al. report tumor control with ^{177}Lu-DOTATATE in a 74-year-old female patient with recurrent and unresectable ONB [27]. Finally, assessing

the degree of Gallium-DOTATATE can be used to predict response to ^{177}Lu-DOTATATE. The Krenning scale, a scale that compares uptake to that of the liver, is used to measure uptake. Lasocki et al. found that if the tumor demonstrates uptake greater than the liver, there is better response to ^{177}Lu-DOTATATE [23].

3D Printing

Imaging of the anterior skull base can be used to construct 3D printed models [28] that can be useful in the care of patients of the anterior skull base for pre-surgical planning, patient education, and trainee education [29].

For use in 3D printing, high-resolution computer tomography or magnetic resonance imaging is acquired in the axial format with thin slices, ideally 0.75 mm or smaller. If obtained with CT, it should be reconstructed and reformatted in the coronal and sagittal planes using a soft tissue algorithm. The images are then imported into a computer-aided design (CAD). At our institution, the CAD program we use is Mimics (Materalise, Plymouth, MI). This image set then undergoes further image transformation, first by a process called segmentation, which defines the anatomic area of interest through both manual and automated thresholding. Next, the raw volumetric data is imported into another image processing program for further refinement of triangular mesh data using smoothing techniques. There are a number of different technologies for printing that vary by the type of material and colors used, cost, and post-production processing [28].

In pre-surgical planning, surgeons have used 3D printed models to assess a proposed surgical corridor approach and determine and potential limitations of exposure that may impact the type of approach taken. In addition, authors have found that the ability to manipulate a model with their hands in 3 dimensions helps them perform surgery with more efficiency and confidence. In trainee education, multiple surgical simulation models have been developed to offer high fidelity models to develop surgical approach and skills. Models have been used to develop endonasal drilling skills [30], and simulate endoscopic carotid injury management [31, 32] and endoscopic pituitary tumor resection [33].

Nasoseptal Flap Enhancement in Post-operative MRI

T1 post gadolinium MRI has been used examine the vascularity of nasoseptal flap in the post-operative setting [34]. Using this imaging technique, a study was able to compare primary nasoseptal flaps to delayed nasoseptal flaps. This imaging supported the conclusion that delayed nasoseptal flaps maintain vascularity and are a viable reconstructive option for sellar and parasellar skull base defects.

Conclusion

CT and MRI are the workhorse imaging modalities of the anterior and central skull base. Together, they help narrow a differential diagnosis and plan treatment. Recent advances in the use of MR elastography, ICG fluorescence, Gallium-DOTATATE, PRRT, and 3D printing show promise in improving the care of patients with pathology of the anterior and central skull base.

Compliance with Ethical Standards

Conflict of Interest Christopher M. Low, Jamie J. Van Gompel, and Garret W. Choby declare that they have no conflict of interest.

Human and Animal Rights and Informed Consent This article does not contain any studies with human or animal subjects performed by any of the authors.

References

Papers of particular interest, published recently, have been highlighted as:
•• Of major importance

1. Iida E, Anzai Y. Imaging of Paranasal sinuses and anterior skull base and relevant anatomic variations. Radiol Clin N Am. 2017;55(1):31–52.
2. Borges A. Imaging of the central skull base. Neuroimaging Clin. 2009;19(3):441–68.
3.•• Wang EW, Zanation AM, Gardner PA, et al. ICAR: endoscopic skull-base surgery. Int Forum Allergy Rhinol. 2019;9(S3):S145–365 **This international consensus guideline critically reviews the literature and provides evidence recommendations for endoscopic skull base surgery including the role of imaging.**
4. Thust SC, Yousry T. Imaging of skull base tumours. Rep Pract Oncol Radiother. 2016;21(4):304–18.
5. Bernstein MA, Huston J III, Ward HA. Imaging artifacts at 3.0 T. J Magn Reson Imaging: An Official Journal of the International Society for Magnetic Resonance in Medicine. 2006;24(4):735–46.
6. Parmar H, Gujar S, Shah G, Mukherji SK. Imaging of the anterior skull base. Neuroimaging Clin. 2009;19(3):427–39.
7. Borges A. Skull base tumours part I: imaging technique, anatomy and anterior skull base tumours. Eur J Radiol. 2008;66(3):338–47.
8. Madani G, Beale TJ, Lund VJ. Imaging of sinonasal tumors. Paper presented at: Seminars in Ultrasound, CT and MRI2009.
9. Francies O, Makalanda L, Paraskevopolous D, Adams A. Imaging review of the anterior skull base. Acta Radiol Open. 2018;7(5): 2058460118776487.
10. Meyers SP, Hirsch W Jr, Curtin H, Barnes L, Sekhar L, Sen C. Chondrosarcomas of the skull base: MR imaging features. Radiology. 1992;184(1):103–8.
11. Meyers SP, Hirsch W, Curtin HD, Barnes L, Sekhar LN, Sen C. Chordomas of the skull base: MR features. Am J Neuroradiol. 1992;13(6):1627–36.
12. Gao A, Bai J, Cheng J, et al. Differentiating skull base chordomas and invasive pituitary adenomas with conventional MRI. Acta Radiol (Stockholm, Sweden : 1987). 2018;59(11):1358–64.

13. Glaser KJ, Manduca A, Ehman RL. Review of MR elastography applications and recent developments. J Magn Reson Imaging. 2012;36(4):757–74.
14.•• Hughes JD, Fattahi N, Van Gompel J, Arani A, Ehman R, Huston J. Magnetic resonance elastography detects tumoral consistency in pituitary macroadenomas. Pituitary. 2016;19(3):286–92 **This study demonstrates the feasibility of determining the mechanical properties of pituitary macroadenomas by magnetic resonance elastography.**
15. Litvack ZN, Zada G, Laws ER. Indocyanine green fluorescence endoscopy for visual differentiation of pituitary tumor from surrounding structures. J Neurosurg. 2012;116(5):935–41.
16.•• Hide T, Yano S, Shinojima N, Kuratsu J-I. Usefulness of the indocyanine green fluorescence endoscope in endonasal transsphenoidal surgery. J Neurosurg. 2015;122(5):1185–92 **This study shows that indocyanine green fluorescence is used in endonasal transsphenoidal surgery to identify vascular srtructures with the goal of preservation the function of critical neuroendocrine structures.**
17. Verstegen MJ, Tummers QR, Schutte PJ, et al. Intraoperative identification of a normal pituitary gland and an adenoma using near-infrared fluorescence imaging and low-dose indocyanine green. Oper Neurosurg. 2016;12(3):260–8.
18. Kerr EE, Jamshidi A, Carrau RL, et al. Indocyanine green fluorescence to evaluate nasoseptal flap viability in endoscopic endonasal cranial base surgery. J Neurol Surg Part B: Skull Base. 2017;78(05):408–12.
19. Lavigne P, Ahmed OH, Gardner PA, Snyderman CH, Wang EW. Indocyanine green fluoroscopy for intraoperative visualization of pterygopalatine fossa vasculature. J Neurol Surg Part B: Skull Base. 2019;80(S 01):P156.
20. Cho SS, Jeon J, Buch L, et al. Intraoperative near-infrared imaging with receptor-specific versus passive delivery of fluorescent agents in pituitary adenomas. J Neurosurg. 2018;1(aop):1–11.
21.•• Hofman MS, Lau WE, Hicks RJ. Somatostatin receptor imaging with 68Ga DOTATATE PET/CT: clinical utility, normal patterns, pearls, and pitfalls in interpretation. Radiographics. 2015;35(2):500–16 **Written close to the time of FDA approval of Gallium-DOTATATE, this study discusses the normal findings of a Gallium-DOTATATE PET/CT scan and suggests the potential utility of this imaging technique.**
22. Ivanidze J, Roytman M, Sasson A, et al. Molecular imaging and therapy of somatostatin receptor positive tumors. Clin Imaging. 2019.
23. Lasocki A, Hicks RJ. How we read: the combined use of MRI and novel PET tracers for the characterisation and treatment planning of masses in neuro-oncology. Cancer Imaging. 2019;19(1):57.
24. Czapiewski P, Kunc M, Gorczyński A, Haybaeck J, Okoń K, Reszec J, et al. Frequent expression of somatostatin receptor 2a in olfactory neuroblastomas: a new and distinctive feature. Hum Pathol. 2018;79:144–50.
25. Makis W, McCann K, McEwan A. Esthesioneuroblastoma (olfactory neuroblastoma) treated with 111In-octreotide and 177Lu-DOTATATE PRRT. Clin Nucl Med. 2015;40(4):317–21.
26. Schneider JR, Shatzkes DR, Scharf SC, et al. Neuroradiological and neuropathological changes after 177Lu-Octreotate peptide receptor radionuclide therapy of refractory esthesioneuroblastoma. Oper Neurosurg. 2018;15(6):100–9.
27. Sabongi JG, Gonçalves MCP, Alves CDC, Alves J, Scapulatempo-Neto C, Moriguchi SM. Lutetium 177-DOTA-TATE therapy for esthesioneuroblastoma: a case report. Exp Ther Med. 2016;12(5):3078–82.
28. Low CM, Morris JM, Price DL, et al. Three-dimensional printing: current use in rhinology and endoscopic skull base surgery. Am J Rhinol Allergy. 2019;33(6):770–81 1945892419866319.
29. Low CM, Morris JM, Matsumoto JS, Stokken JK, O'Brien EK, Choby G. Use of 3D-printed and 2D-illustrated international frontal sinus anatomy classification anatomic models for resident education. Otolaryngol Head Neck Surg. 2019;161(4):705–13.
30. Lin J, Zhou Z, Guan J, et al. Using 3D printing to create individualized cranial nerve models for skull base tumor surgery. World Neurosurgery. 2018;16:16.
31. Maza G, VanKoevering KK, Yanez-Siller JC, et al. Surgical simulation of a catastrophic internal carotid artery injury: a laser-sintered model. Int Forum Allergy Rhinol. 2019;9(1):53–9 0(0).
32. Muto J, Carrau RL, Oyama K, Otto BA, Prevedello DM. Training model for control of an internal carotid artery injury during transsphenoidal surgery. Laryngoscope. 2017;127(1):38–43.
33. Wen G, Cong Z, Liu K, et al. A practical 3D printed simulator for endoscopic endonasal transsphenoidal surgery to improve basic operational skills. Childs Nerv Syst. 2016;32(6):1109–16.
34. Choby GW, Mattos JL, Hughes MA, et al. Delayed nasoseptal flaps for endoscopic skull base reconstruction: proof of concept and evaluation of outcomes. Otolaryngol Head Neck Surg. 2015;152(2):255–9.